NASA Technical Memorandum 103648

Effect of Fiber Reinforcements on Thermo-oxidative Stability and Mechanical Properties of Polymer Matrix Composites

Kenneth J. Bowles
Lewis Research Center
Cleveland, Ohio

January 1991

NASA

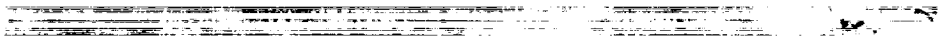

EFFECT OF FIBER REINFORCEMENTS ON THERMO-OXIDATIVE STABILITY AND MECHANICAL PROPERTIES OF POLYMER MATRIX COMPOSITES

Kenneth J. Bowles
National Aeronautics and Space Administration
Lewis Research Center
Cleveland, Ohio 44135

ABSTRACT

A number of studies have investigated the thermo-oxidative behavior of polymer matrix composites. Two significant observations have been made from these research efforts. First, fiber reinforcement has a significant effect on composite thermal stability; second, geometric effects must be considered when evaluating thermal aging data. A number of studies that address these areas have been performed at the NASA Lewis Research Center. The information presented herein, a compilation of some results from these studies, shows the influence of the reinforcement fibers on the oxidative degradation of various polymer matrix composites. The polyimide PMR-15 was the matrix material that was used in these studies. The control composite material was reinforced with Celion 6000 graphite fiber. T-40R graphite fibers, along with some very stable ceramic fibers were selected as reinforcing fibers because of their high thermal stability. The ceramic fibers were Nicalon (silicon carbide) and Nextel 312 (alumina-silica-boron oxide). The mechanical properties of the two graphite fiber composites were significantly different, probably owing to variations in interfacial bonding between the fibers and the polyimide matrix. The Celion 6000/PMR-15 bond is very tight, but the T-40/PMR-15 bond is less tight. Three oxidation mechanisms were observed. One involved the preferential oxidation of the Celion 6000 fiber ends at cut surfaces, leaving a surface of matrix material with holes where the fiber ends were originally situated; the second, preferential oxidation of the composite matrix; and the

third, interfacial degradation by oxidation. The latter two mechanisms were also observed on fiber end cut surfaces. The fiber and interface attacks appeared to initiate interfiber cracking along these surfaces.

Keywords: Composites, polyimides, aging, graphite fiber, oxidation, interfaces, mechanical properties

INTRODUCTION

A number of studies have investigated the thermo-oxidative behavior of polymer matrix composites [1-7]. Two significant observations have been made from these research efforts. First, fiber reinforcement has a significant effect on composite thermal stability [1-5], and second, geometric effects must be taken into consideration in evaluating thermal aging data [4-7].

At the time this series of studies was conducted, it appeared that Celion 6000 would be the standard reinforcement for high-temperature polyimide composites because it imparts excellent mechanical properties to the composites. As time progressed, graphite fibers more thermally stable than Celion 6000 were made available. The consensus was that these fibers should produce a more thermally stable composite than the Celion 6000/PMR-15 control and therefore could be considered for future use in high-temperature structures. As a result of this thinking, the thermally stable T-40R fibers, along with some very stable ceramic fibers were selected for high-temperature air aging studies in PMR-15 composites. Nicalon (silicon carbide) and Nextel 312 (alumina-silica-boron oxide) were the ceramic fibers that were selected.

A number of polymer matrix composite thermo-oxidative stability studies that address these areas have been carried out at the NASA Lewis Research Center [1,4-7]. The information presented herein is a compilation of some results from these studies that show how reinforcement fibers influence the oxidative degradation and mechanical behavior of various polymer matrix composites.

MATERIALS

Only one matrix, the polyimide PMR-15, was used in these studies. The formulation of the monomers and the processing of the composites are adequately

described elsewhere [8]. All the laminates that were studied were unidirectional composites made from prepreg tape. The control material was reinforced with Celion 6000 graphite fiber. Except for the Nextel 312 fiber and some Nicalon fibers, all the fibers that were studied were unsized. The Nextel fiber was sized with A-1100 sizing (silane sizing). The Nicalon fiber was received in two batches. The first batch was sized with polyvinyl acetate (PVA). Some composites were processed with this sized fiber, and some composites were processed with fibers that had been stripped of the sizing with acetone in an ultrasonic bath. A second batch of Nicalon fiber was received with a bismaleimide-compatible sizing (BMIC), and this fiber was also tested.

Figure 1(a) is a schematic illustrating the different types of surfaces that are present on a machined, continuous-fiber-reinforced composite. S1 denotes the resin-rich surface that contacts the matched metal die mold surfaces. S2 is the surface produced by cutting the composite parallel to the fiber axes, and S3 is the surface produced by cutting the composite perpendicular to the fiber axes. Also shown (Fig. 1(b)) is a micrograph of an aged composite that was cut parallel to the fiber axes. The inner core of the composite (the dark area) has not been oxidized. Surrounding this core on the top, bottom, and left are layers of the composite that were degraded by a limited amount of oxidation (light area) controlled by diffusion of oxygen into the composite. The surfaces shown in this figure are referred to throughout this article.

FIBERS

The chemical composition, including some trace elements, of the four fibers that were used as composite reinforcements in these studies are listed in Table 1 and the fiber properties are listed in Table 2. The analyses were done using atomic spectra measurements of the bulk fiber. Figure 2 shows

scanning electron micrographs of the circumferential surfaces of the four fibers. The surface features of the two ceramic fibers differed significantly from those of the graphite fibers. The ceramic fibers exhibited a topographically smoother but more grainy surface than the graphite fibers, with the Nextel 312 fibers having a much rougher surface than the Nicalon fibers. The graphite fibers (Figs. 2(a) and (b)) had striations on the surfaces, which ran parallel to the fiber axes. The amount and size of the striations appeared to be about the same for both the Celion 6000 and the T-40R fibers.

Surface areas, measured by using the Brunauer-Emmet-Teller isotherm analysis (BET) with krypton as the gas, were 3.99 and 5.5 cm^2/mg for the Celion 6000 and T-40R fibers respectively. Eckstein [9] measured values of 4.4 and 5.5 cm^2/mg for the same two fibers. Calculated surface areas, based on density and average diameter values, for the two fibers were 3.15 cm^2/mg for Celion 6000 and 2.26 cm^2/mg for T-40R. The deep striations in the T-40R fiber actually increased the surface area to almost 2.5 times the calculated area for a fiber with a smooth surface.

The measured T-40R fiber surfaces were about 35 percent greater than those of the Celion 6000 control reinforcement. None of this difference can be attributed to differences in surface features. However, because the T-40R fiber has a smaller diameter than the Celion 6000 fiber, it has about 37 percent more surface area per unit weight (or volume, since they both have the same density). The diameter difference appears to be the significant factor in the difference in graphite fiber surface areas.

One very important difference between the two graphite fibers is the amount of measured BET porosity that is exposed as the aging time in air increases. This is illustrated in Figure 3, which shows a plot of exposed fiber surface area as a function of fiber weight loss for both graphite fibers.

The rapid increase in surface area for the Celion 6000 fiber shown in the figure is accompanied by a similar increase in porosity measuring 50 Å in diameter. The BET data suggest that a Celion 6000 fiber consists of a thin, oxygen-impervious outer shell surrounding a porous core. One fact that must be noted from the data in Table 2 is that the densities of the two graphite fibers are almost the same. Therefore, it can be speculated that other structural differences must exist in the two fibers.

References [9-13] propose that carbonized fibers have the ribbon-like structure shown in Figure 4. As the fibers are heat treated to higher temperatures, the ribbons straighten out and the open spaces between them become smaller. Brown and Phillips [14] found that carbonized fibers with a tensile modulus of elasticity of 690 GPa (40 Msi) consist of 40-Å-wide ribbons. The voids can be about the size of those measured by BET techniques in this study. Reference [14] also reports that the ribbons closest to the outer surface of a fiber are more highly oriented than those near the center. Thus, the outer skin of lower-modulus fibers should be less porous than the fiber core. Also lower-modulus fibers should show a more rapid loss in weight and mechanical properties than the higher-modulus fibers as the aging time in air increases because the lower-modulus fibers have less basal plane alignment on the circumferential surfaces. Basal planes contain the fewest active sites of any planes of the carbon cell. Therefore, more active sites are available for oxidative attack on the surfaces of the lower-modulus fibers than on the surfaces of the higher-modulus fibers [15].

One final difference between the two graphite fibers that were studied was the concentration of free radicals within the fibers. Electron spin resonance (ESR) measurements indicated that the Celion 6000 fiber had a high concentration of free radicals but that the T-40R fiber contained almost no

free radicals. ESR measurements were made of the as-received fibers and also of fibers that were ground in ball mills. No changes in free radical concentration between the milled and unmilled fibers were measured. For this reason and since the surface area of the graphite was increased tremendously from the milling process, it can be assumed that the free radicals were not concentrated on the Celion 6000 surfaces but were evenly distributed throughout the fiber.

Nicalon is a silicon-carbon-oxygen fiber that is derived from methylpolysilane [16]. It contains 15 wt% oxygen. The surface is smooth and impervious (Fig. 2(c)). A variety of surface-connected porosity techniques, such as BET adsorption-desorption and mercury porosimetry, indicate that the measured surface area is close to the calculated area of 1.56 cm^2/mg [18]. Calculations using the rule of mixtures based on volume additivities for components in their appropriate states indicate that these fibers do contain about 16 percent porosity [18]. Little or no surface porosity is present, however. Therefore it is assumed that all the porosity is confined to the interior of the fiber.

The nominal chemistry of the Nextel 312 fiber is 62 wt% Al_2O_3, 24 wt% SiO_2, and 14 wt% B_2O_3. A comparison of the measured density (2.7 to 2.9 g/cm^3) with the calculated density (3.36 g/cm^3) indicates a 17 percent void content. It is assumed that the voids are similar to those described for Nicalon fibers. The Nextel 312 fiber (Fig. 2(d)) appears to have a rougher surface than the Nicalon fiber. The roughness is probably due to the size of the alumina crystallites. Normal sintering conditions for alumina lead to small grain size but also to pore growth [19]. Silica is added to the alumina to increase the crystallinity and the crystallite size and also to decrease the porosity. A tradeoff between crystallite size and porosity is apparently necessary. The

Nextel 312 fiber cross section is oval, rather than round like those of the other three fibers. The major diameter is twice the minor diameter [21]. The surface area is <2.0 cm^2/mg, which is the calculated geometric area [20].

MECHANICAL PROPERTIES

Table 2 lists the mechanical properties of the four fibers. The Nextel 312 fiber has the lowest tensile strength, tensile modulus, and strain to failure of the four reinforcements. This may be due to the grained texture of the surface (see Fig. 2(d)) or high concentrations of a constituent in the grain boundaries. The grain boundaries may be considered to be surface defects that act as stress risers to cause failure below the normal strength value for the bulk material.

Table 3 presents the composite mechanical properties for laminates that are reinforced with the four fibers. Included in the table is a column with the heading "Flexural strength (rule of mixtures)." The flexural strengths in this column are 1.5 times the calculated rule-of-mixtures tensile strengths of the composites [10]. The effectiveness of translating fiber properties to composite properties is shown in the column entitled "(Measured/Calculated) 100." This is the measured value divided by the rule-of-mixtures value expressed in percentages. Except for the Celion 6000 and the Nicalon (BMIC)-reinforced composites, the effectiveness was between 44 and 49 percent. The Celion 6000-reinforced composites, 90.0 percent, and the Nicalon (BMIC)-reinforced composites, 90.8 percent, have much larger conversions. Table 3 also shows that the Nicalon (BMIC) reinforcement imparted the greatest flexural strength and interlaminar shear strength (ILSS) to the processed composites.

AIR AGING BEHAVIOR

Graphite Fibers

The composites that were studied differed significantly in air aging behavior. It is quite interesting that major differences in the effects of high-temperature exposure to air even existed between the two graphite fibers. These differences are presented in this section.

The relationship between weight loss rate and aging time at 316 °C for the two bare graphite fibers are shown in Figure 5. It is evident that the T-40R fiber is much more thermally stable than the Celion 6000 fiber. Data for the bare ceramic fibers are not included in this figure since, naturally, the fibers exhibited no significant weight changes, except for sizing deterioration, under these conditions.

The 316 °C air aging weight loss history for aging times less than 1000 hours is shown for each of the six PMR-15 composites in Figure 6. The thermo-oxidative stability of the fibers is not reflected in the composite stability. The least thermally stable fiber, the Celion 6000 fiber, produced the most thermally stable composite. The most thermally stable ceramic fibers did not impart their stability to the PMR-15 composites. They were the least stable composites.

The geometry of the Celion 6000/PMR-15 composites substantially affects the weight loss rate [5,6]. The geometric effects were found to be due to excessive weight loss from the cut specimen edges. The edge effects were enhanced by the development of cracks in the edges. The cracks developed and increased as the aging time progressed. The T-40R-fiber-reinforced composites show no geometry effects initially, but after about 400 hours geometry effects become apparent [7]. (See Fig. 7.) The ceramic-fiber-reinforced composites are reported to show no geometry effects at all [7].

The most rapid oxidation attack on the Celion 6000/PMR-15 composite is along the S3 surfaces, those cut perpendicular to the fiber axes [5]. The oxidation caused intralaminar cracking that advanced parallel to the fibers and into the laminate specimen as time progressed. The damage is shown in Figure 8(a). Similar cracks were observed in the ceramic composites. In contrast, no S3 surface cracks were observed in the T-40R/PMR-15 composite (Fig. 8(b)).

Larger magnifications of Figure 8 are shown in Figure 9. Figure 9(a) shows the end view (surface S3) of a Celion 6000 fiber in a PMR-15 composite. The fiber end exhibits a very erosive surface, one with edges that appear to be worn smooth. The fiber cracked into distinct, separate pieces. Although the fiber circumferential surfaces were protected from oxidation by the matrix during air aging, the end cracking allowed access to the inner, porous core of the fiber.

Note that degradation of the fiber-matrix interface is also apparent in Figure 9(a), as evidenced by the space between the matrix and the fiber. Fiber diameter measurements from scanning electron micrographs indicate that the fiber was degrading, resulting in a reduction in the fiber diameter. The diameter of the resultant hole in the matrix remained the same as the initial fiber diameter.

The typical appearance of air-aged fibers, along the S2 surface at a location away from the fiber ends (S3 surface), is shown in Figure 10. Deep striations developed along the surface and parallel to the fiber axis. These striations were much more pronounced than those on the surface of the Celion 6000 shown in Figure 2.

Even the surfaces of the fibers that were in parts of the composite which are not directly exposed to the air underwent changes from thermal exposure

alone. Figures 11(a) and (b) show a fiber end surface and a fiber circumferential surface that are located in the degraded outer layer shown in Figure 1. In both cases there appeared to be a coating over the normally smooth fiber surfaces. The texture of the surfaces resembled that of an ear of corn. When the composite was digested to measure the fiber fraction, or when the surface was exposed to air at an elevated temperature, this surface texture disappeared, leaving the normal surface shown in Figure 10. These figures suggest that a reaction product forms at the fiber-matrix interface at 316 °C under anaerobic conditions and that the reaction products disappear when exposed to oxidizing conditions. One item of interest in Figure 11(a) is that the fiber appears to be made up of small fibrils about 0.4 μm in diameter.

Figure 9(b) shows the end of a T-40R fiber that was exposed to 316 °C air at the cut S3 surface of a PMR-15 composite. The matrix surface receded leaving the T-40R fibers exposed like whiskers. The surface of the cut fiber has the texture of ground meat. The strings are called radials and the sharpness of the micrograph indicates that air aging had no obvious effects on the exposed end surfaces of the T-40R fibers. Corners are not rounded and surface contours are not smoothed out. In another area of the T-40R/PMR-15 composite, shown in Figure 12, preferential oxidative attack has occurred in the matrix. The fibers are surrounded by what looks like relatively less aggressively oxidized layers of matrix material, measured to be 1.5 μm thick, that form sheaths around the fibers. The matrix material outside of these sheaths and between them, with a tricuspid shape, appears to have been more aggressively attacked by the air than the sheaths. The penetration is deeper and the material has a spongy, void-dominated appearance. It also appears that there are separations between the fibers and the matrix.

These comparisons between the two graphite-fiber-reinforced PMR-15 composites do point out substantial differences in their behavior under oxidizing conditions. In one case (Celion 6000), the fibers oxidized preferentially and receded beneath the surface of the composite, leaving only the matrix exposed and apparently unattacked, or much less degraded than the fiber. In the other case (T-40R), the matrix was more rapidly attacked and it receded, leaving whiskers of relatively unattacked fibers at the surface of the oxidized composite.

In order to look more closely into the origin of the voids in the matrix outside of the sheath material that surrounds the T-40R fibers in Figure 12, air-aged specimens of T-40R/PMR-15 composites were cut to expose their interiors. The specimen interiors were protected from direct contact with the environment. The two scanning electron micrographs of the specimen in Figure 13 show T-40R graphite fibers surrounded by the PMR-15 matrix. The specimen was mounted in a metallographic mount and polished. Very small voids are visible, but there are no signs of matrix differences that would indicate the presence of sheaths around the fibers. One item of significance is the presence of a separating crack or the concentration of voids at the interface in the micrographs. Also note how flat the fiber surfaces are from polishing.

For purposes of comparison with the T-40R-fiber-reinforced composite shown in Figure 13, the same type of polished specimen was prepared from a Celion 6000-reinforced composite specimen. The fiber surface and the matrix surface, as shown in Figure 14, appear different from the T-40R fiber and matrix shown in Figure 13. The matrix exhibits more grainy features and the fiber surface contains a significant amount of relief with small hills and valleys in evidence. No separation is visible between the fiber and the matrix.

Ceramic Fibers

The difference between the oxidation of composites reinforced with ceramic fibers and those reinforced with graphite fibers is illustrated in Figure 15, which shows the S3 surfaces of the Nicalon and Nextel 312 composites. The oxidative attack was concentrated in the matrix, but there was no preferential oxidative attack like that on the T-40R composite. Figure 15 shows significant separations between the PMR-15 matrix and the Nicalon and Nextel 312 fibers. The width of the separations was estimated to be about 0.5 μm.

The extent of interfacial bonding between the ceramic fiber and the polyimide matrix is illustrated in Figure 16, which shows the fiber surfaces of a composite specimen that was cleaved parallel to the fibers. Note that no particles of the matrix are attached to the fiber surfaces. This indicates poor bonding at the interface all along the fibers, and not just at the S3 surfaces as shown in Figure 15.

Figure 17 shows the interior of a Nicalon/PMR-15 composite and is a typical micrograph of the interfacial features of all ceramic/PMR-15 composites including the Nicalon (BMIC)-reinforced composite. There is no evidence of matrix oxidation along the interface in the interior of the composite. All the weight loss appears to be confined to the exterior surfaces of ceramic-fiber-reinforced composites.

DISCUSSION

One of the most important conclusions gleaned from the studies done at the NASA Lewis Research Center is that the thermal stability of the fibers is not the dominant factor in determining composite stability. The reason for this is that the fiber-matrix interface plays such an important role in both the thermal and mechanical behavior of polymer matrix composites.

The substantial difference between the mechanical properties of composites with each of the two graphite fibers as the reinforcing material is probably due to the degree of observed bonding between the fibers and the polyimide matrix. In Figure 11 the bond between the Celion 6000 and the PMR-15 appears to be very tight. On the other hand, due to fiber-matrix separations (Fig. 13), the T-40R/PMR-15 interfacial bond appears to be less tight. Although the T-40R fiber has a slightly rougher surface and larger surface area per unit weight than the Celion 6000 fiber, the transfer of loads from the fiber to the resin matrix was more efficient for the Celion 6000 fiber. So, for this case, surface area differences and the resultant proposed mechanical bonding differences were not a significant factor in influencing composite mechanical properties. One may reasonably speculate that the superior properties of the Celion 6000 composite are due to chemical bond interactions between the fiber and the matrix.

Except for the BMIC-sized Nicalon-reinforced composite, the inadequate bonding that caused the ceramic composites to have low mechanical properties was probably due to the lack of a suitable sizing that can sustain the processing temperature of 316 °C as well as due to the fiber surface, which was significantly smoother than the surfaces of the graphite fibers. The BMIC-sized Nicalon-reinforced composite exhibited superior room-temperature mechanical properties, probably because the sizing withstood the processing temperature for the required time and promoted a good interfacial bond. The results of the thermal aging tests indicate that this bonding broke down after extended periods at 316 °C, since the weight loss rate did not differ significantly from those of the other Nicalon composites.

The information provided by Figures 9, 13, and 14 indicates that the two graphite fibers have different structures. The BET data indicate a sheath-core

structure for both graphite fibers, with the Celion 6000 fiber possessing a thin sheath and a porous core. The contrast between Figures 13 and 14 indicates that the T-40R fiber (Fig. 13) may have a more uniform structure and therefore a more evenly polished surface than that of the Celion 6000 fiber (Fig. 14). The surface relief shown in the latter figure appears to be a less severe condition than that of the oxidized Celion 6000 fiber shown in Figure 9(a), but one that can be imagined to be the onset of a transformation into a final appearance similar to it.

Microstructural characterization has been performed on a number of graphite fibers including Celion 6000 and T-40R [14]. It was found that the fibers have two different cored structures. The Celion fiber has a three-zone structure. Brown and Phillips [14] propose the outer zone to be a smooth laminar phase with the 0002 planes oriented as a smooth cylindrical sheath parallel to the fiber surface. They consider a second phase within the outer sheath to be a rough laminar phase that has the 0002 planes as small crystallites containing parallel and flat planes. The crystallites are oriented somewhat parallel to the fiber surface and they are likely to intersect the surface at an oblique angle. They describe the central core, or third phase, as turbostratic. In a turbostratic carbon structure, the 0002 planes are oriented roughly parallel to the fiber axes and random within a plane perpendicular to the fiber axes. For a more complete description see Reference [14].

Brown and Phillips [14] propose the T-40R fiber to have a two-zone structure with the outer zone being a smooth laminar sheath and the inner phase being rough laminar. From a comparison of the two proposed structures and the results of the BET analyses for the graphite fibers, it could be inferred that the turbostratic carbon structure is the porous structure. The data presented

in Reference [14] confirm this inference, since the density listed for the Amoco WCA fiber (a turbostratic fiber) is 1.47 gm/cm^3, in contrast to 1.78 and 1.81 gm/cm^3 for the Celion 6000 (G30-500) and T-40R fibers, respectively. One inconsistency remains. The celion 6000 and the T-40R fibers have the same density. The apparent low density of the turbostratic structure in the T-40R fiber is not reflected in the density of the T-40R fiber.

The following hypothesis can be made from the visible evidence of bonding between the two constituents of the graphite composite: The more rapid oxidation of the fibers in the Celion 6000-reinforced composite causes the fibers to recede into the composite, and the stored strain energy in the matrix may result in matrix cracking along the S3 surfaces. In contrast, the strained matrix in the T-40R-reinforced composite is oxidized away, leaving only exposed fibers with no matrix cracking. One can consider that the S3 surface appearance depends both on the degree of bonding between the fiber and the matrix and on the relative thermal stability of the resin and the fiber.

There is one other consideration that is not addressed by the observations presented herein. That is the possibility of chemical composition changes in the matrix as the distance from the fiber surface increases. The composition at the interface may be influenced by the reinforcement. Other than the more aggressive oxidation of the matrix away from the fiber surfaces that is shown in Figure 12, no other evidence of compositional differences is available from this study.

Another area of great interest is the tricuspid-shaped region of the S3 surface of the oxidized T-40R-reinforced composite that is shown in Figure 12. This region of the matrix looks as if it were more aggressively oxidized than the matrix adjacent to the fibers. The distribution of shrinkage stresses in the matrix was such that the compressive radial stresses and the hoop stresses

decreased as the distance from the fiber surface increased. This tricuspid-shaped region between the triangular array of fibers is an area of lower stresses than the area of the matrix adjacent to the fibers [15,16]. For the T-40R-reinforced composite, the difference in oxidation rate shown in Figure 12 may be stress induced. It would be of value to the understanding of composite thermal stability to experimentally explore the effect of stress on the polymer oxidation rate. The limited amount of effort expended in this study indicates that a carefully thought out program is required. It would also be beneficial to determine failure envelopes by conducting creep rupture experiments in oxidative and inert atmospheres.

The ceramic-fiber-reinforced composites that were studied appear to have oxidized at the S3 surfaces, in general, by a mechanism similar to that experienced by the T-40R graphite composites. Rather than a selective oxidation in the fiber or the matrix, the composite degradations appeared to take place at the ceramic-polymer interfaces as shown by the interfacial gaps in Figures 14 and 15. Because these gaps did not extend for a significant distance into the composites, they could not have been caused by unequal shrinkage of the composite constituents during cooldown after curing. Figure 17 shows a cross section of the interior of an aged ceramic-fiber-reinforced composite. There are no interfacial gaps. It appears that at least a satisfactory mechanical bond existed in the bulk of the ceramic composites. The evidence indicates that there is a good probability that the concentrated oxidation at the interfaces may have been caused by a concentration of light metal atoms at the surfaces of the ceramic fibers [2]. The surface chemistry of all the fibers (Table 1) shows that the light-metal concentration was greater on the ceramic fibers than on the graphite fibers.

Reference [7] states that the extreme amount of S3 surface cracking and erosion-like attack observed in Celion 6000 composites does not occur in the ceramic composites. Some cracking did occur in the S3 surfaces of the Nextel 312 composites, as evidenced in Figure 18. The presence of these cracks support the theory that crack formation in the S3 surfaces of the Celion 6000 composites may be caused by the stress gradient parallel to the fibers. The gradients are set up in the matrices of these composites when the shrinkage mismatches between the ceramic fibers and the polymer matrices release residual stresses. As shown in Figure 15, the ceramic fibers show no signs of interfacial bonding at the exposed ends of the fibers. This is evidenced by the presence of gaps between the fibers and the matrix in both ceramic composites. The situation is the same as with the Celion 6000 composite, and some cracking in the ceramic composites would therefore be reasonable.

Figure 14 with Figure 11, reveals a distinct, continuous interface between the Celion 6000 graphite fiber and the PMR-15 matrix. From this evidence and the fiber surface micrographs shown in Figures 9 to 11, it may be speculated that a reaction zone formed at the Celion 6000/PMR-15 interface in the degraded surface zones of the composite during air aging at 316 °C. This zone may not be distinct in Figure 14 but may merge the fiber with the matrix through a gradient of reaction products that changes in composition from polyimide to graphite over the width of the zone. The formation of this zone changes the Celion 6000 fiber shape from circular to striated circular (Fig. 10). This zone, which may be the surface material in Figure 11, maintains the interfacial bond to allow acceptable retention of mechanical properties during the air aging of this material.

CONCLUSIONS

The following conclusions were drawn from the results of this study:

1. Fiber thermal stability is not translated into composite stability.

2. Bonding forces are more important than fiber surface area and topography in establishing fiber-matrix bond efficiency.

3. Ceramic fibers and thermally stable graphite fibers may require high-temperature sizing to promote sufficient interfacial bonding to provide good mechanical properties and thermal stability to their composites. However, light-metal concentrations at the fiber-matrix interface, from sizings, could enhance oxidation in this area.

4. Fiber chemical composition and graphite structure influence fiber and composite thermal stability. The amount of light-metal elements, such as Na and Ca, appear to significantly decrease polymer matrix composite thermal stability.

ITEMS FOR FUTURE STUDY

The following observations were made during this study and efforts should be made to investigate them further:

1. Celion 6000 fibers and PMR-15 polyimide may react at their interface during thermal aging.

2. The carbon structure in the Celion 6000 fiber appears to change during aging. The fiber seems to transform into a nonhomogeneous material with varying degrees of hardness across the diametral cross section.

3. The effect of stresses on the thermal behavior of polymers may be significant.

4. Oxidation mechanisms may generate thermal stress gradients that can cause composite cracking and enhanced oxidation which would be significantly influenced by geometry factors.

REFERENCES.

1. Hanson, M.P., and Serafini, T.T. "Effects of Thermal and Environmental Exposure on the Mechanical Properties of Graphite/Polyimide Composites," Space Shuttle Materials; Proceedings of the National Technical Conference, Huntsville, AL, Oct. 5-7, 1971, SAMPE, pp. 31-38 (1971).
2. Gibbs, H.H., Wendt, R.C., and Wilson, F.C. "Carbon Fiber Structure and Stability Studies," Reinforced Plastics/Composites Institute, Annual Conference, 33rd, Washington, D.C., Feb. 7-10, 1978, Proceedings, New York. The Society of Plastics Industry, pp. 24F1-24F9 (1978).
3. Eckstein, B.H. "Oxidation of Carbon Fibres in Air Between 230° and 375 °C." Fibre Sci. Technol., 14: 139-156 (Oct. 1981).
4. Scola, D.A. "Thermo-Oxidative Stability of Graphite Fiber/PMR-15 Polyimide Composites at 350 °C," High Temperature Polymer Matrix Composites, NASA CP-2385, pp.217-242 (1985).
5. Bowles, K.J., and Meyers, A.E. "Specimen Geometry Effects on Graphite/PMR-15 Composites During Thermo-Oxidative Aging," Materials Science for the Future, International SAMPE Symposium and Exhibition, 31st, J.L. Bauer and K. Dunaetz, eds., SAMPE, pp. 1285-1299 (1986).
6. Bowles, K.J., and Nowak, G. "Thermo-Oxidative Stability Studies of Celion 6000/PMR-15 Unidirectional Composites, PMR-15, and Celion 6000 Fiber," J. Compos. Mater., 22: 966-985 (Oct. 1988).
7. Bowles, K.J. "Thermo-Oxidative Stability Studies of PMR-15 Polymer Matrix Composites Reinforced With Various Continuous Fibers," Advanced Materials: The Challenge for the Next Decade, International SAMPE Symposium and Exhibition, 35th, G. Janicki, V. Bailey, and H. Schjelderup, eds., SAMPE, pp. 147-161 (1990).

8. Vannucci, R.D. "PMR-15 Polyimide Modifications for Improved Prepreg Tack," Proceedings of the 1982 National Technical Conference: The Plastic's ABC's, Society of Plastics Engineers, pp. 131-133 (1982). (NASA TM-82951, 1982).

9. Eckstein, B.H. "The Weight Loss of Carbon Fibers in Circulating Air," Materials Science for the Future, International SAMPE Technical Conference, 18th, Proceedings, J.L. Bauer and R. Dunaetz, eds., SAMPE, pp. 149-160 (1986).

10. Lubin, G., ed. Handbook of Composites. Van Nostrand Reinhold Co., pp. 196-209 (1982).

11. Watt, W., and Perov, B.V., eds. Handbook of Composites, Volume 1-Strong Fibers, North Holland (1985).

12. Fitzer, E., and Weiss, R. "Surface Treatment of Carbon Fibers," Processing and Uses of Carbon Fibre Reinforced Plastics, Duesseldorf, VDSI-Verlag GmbH, pp. 45-64 (1981).

13. Drzal, L.T., Rich, M.J., and Lloyd, P.F. "Surface Treatment Effect on Fiber Adhesion," J. Adhesion, 16: 1-30 (1982).

14. Brown, D.K., and Phillips, W.M. "Effects of Heat Treatment on Carbon Fibers," SAMPE J., 26: 9-13 (Sept.-Oct. 1990).

15. Favre, J.P. "Residual Thermal Stresses In Fibre Reinforced Composite Materials. A Review," J. Mech Behav. Mater., 1: 37-53 (1988).

16. Nairn, J.A. "Thermoelastic Analysis of Residual Stresses in Unidirectional, High Performance Composites," Polym. Compos., 6: pp. 123-130 (Apr. 1985).

17. Bowles, K.J. "A Thermally Modified Polymer Matrix Composite Materia With Structural Integrity to 371 °C," Materials-Processes: The Intercept Point, Proceedings of the Twentieth International SAMPE Technical Conference, SAMPE, pp. 552-561 (1988).

18. Lipowitz, J., Rabe, J.A., Frevel, L.K., and Miller, R.L. "Characterization of Nanoporosity in Polymer-Derived Ceramic Fibers by X-Ray Scattering Techniques," J. Mat. Sci., 25: 2118-2124 (Apr. 1990).

19. Holtz, A.R., and Grether, M.F. "High Temperature Properties of Three Nextel Fibers," Advanced Materials Technology '87, International SAMPE Symposium and Exhibition, 32nd, Proceedings, SAMPE, pp. 245-256 (1987).

20. Watt, W., and Perov, B.V. Strong Fibres: Elsevier Science Publ., pp. 124-130 (1985).

TABLE 1. - SURFACE CONCENTRATION OF ELEMENTS ON GRAPHITE AND CERAMIC FIBERS

Fiber	Carbon	Silicon	Al_2O_3	SiO_2	B_2O_3	Na	Ca	K	Fe
	Concentration, percent					Concentration, ppm			
Celion 6000	95.6	(a)	(a)	(a)	(a)	95	290	22	11
T-40R	98.9	(a)	(a)	(a)	(a)	4	7	1.2	(a)
Nicalon	28.4	55.5	(a)	---	(a)	600	200	(a)	300
Nextel 312	(a)	(a)	62	24	14	2100	200	10	50

[a]Not applicable.

TABLE 2. - FIBER PROPERTIES

Fiber	Tensile strength		Tensile modulus		Strain to failure, percent	Density, g/cm^3	Fiber diameter, μm
	MPa	ksi	GPa	Msi			
Celion 6000	3890	550	235.2	34	1.65	1.78	7.1
T-40R graphite	3640	528	296.5	43	1.23	1.81	5.1
Nicalon	2700	400	200	29	1.38	2.55	10-15
Nextel 312	1380-1724	200-250	151.7	22	0.91-1.14	2.7	10-12

TABLE 3. - PMR-15 MATRIX COMPOSITE ROOM TEMPERATURE MECHANICAL PROPERTIES

Fiber[a]	Property									
	Flexural strength		Flexural strength (rule of mixtures)		$\left(\frac{\text{Measured}}{\text{Calculated}}\right)100$, percent	Flexural modulus		Interlaminar shear strength		Fiber volume, percent
	GPa	ksi	GPa	ksi		GPa	Msi	MPa	ksi	
Celion 6000 (U)	1.86	270.0	2.10	300.0	90.0	113.9	16.3	103.4	15.0	60.0
T-40R (U)	.88	128.0	2.02	294.1	43.5	75.0	10.9	75.0	10.9	55.7
Nicalon (S)	1.0	147.3	2.17	315.6	46.0	88.0	12.8	35.6	5.2	52.6
Nicalon (PVA)	.9	129.0	2.03	294.9	44.4	61.0	8.8	35.6	5.2	49.0
Nicalon (BMIC)	2.05	296.8	2.26	330.0	90.8	105.0	15.0	118.4	16.2	55.0
Nextel 312 (A-1100)	.05	72.5	1.02	147.6	48.5	28.5	4.1	45.8	6.6	49.2

[a]Unsized, U; stripped of sizing with acetone, S; sized with polyvinyl acetate, PVA; bismaleimide-compatible sizing, BMIC; A-1100 sizing, A-1100.

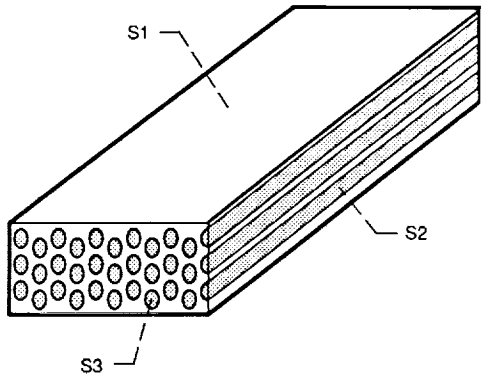

(a) Different types of surfaces.

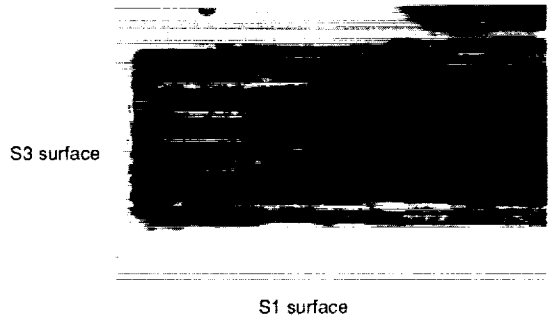

(b) Aged composite cross section showing degraded outer area. Inner dark area is undegraded.

Figure 1.— Composite surfaces.

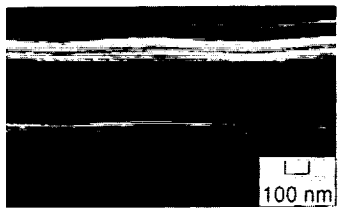

(a) Celion 6000.

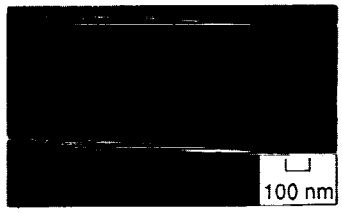

(b) T–40R.

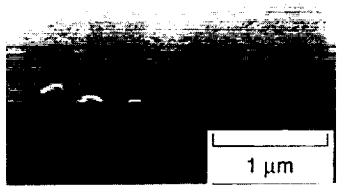

(c) Nicalon.

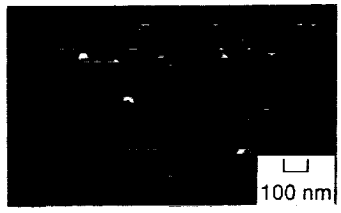

(d) Nextel 312.

Figure 2.—Surfaces of fibers that were studied.

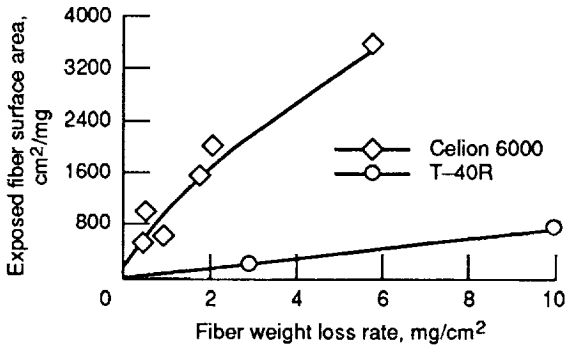

Figure 3.— Exposed surface area as function of weight loss rate for graphite fibers.

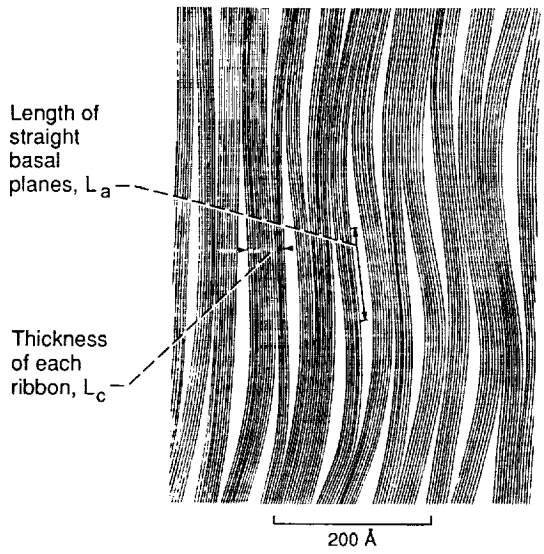

Figure 4.— Model of carbon fiber ribbon structure [10].

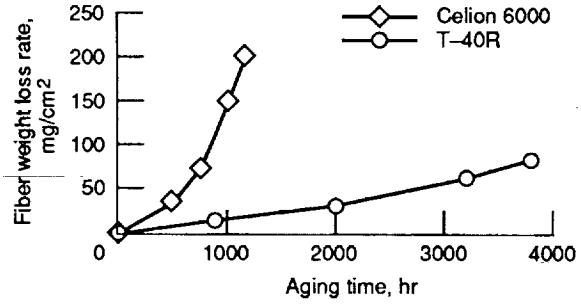

Figure 5.— Weight loss rate of graphite fibers aging in air at 316 °C.

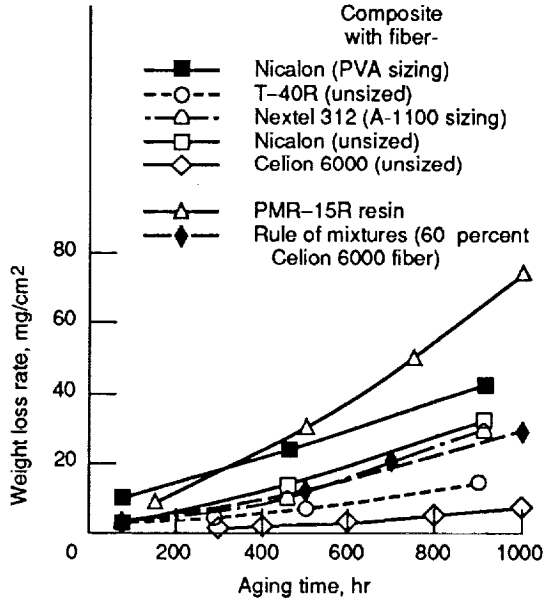

Figure 6.—Weight loss rate of PMR-15 composites aging in air at 316 C.

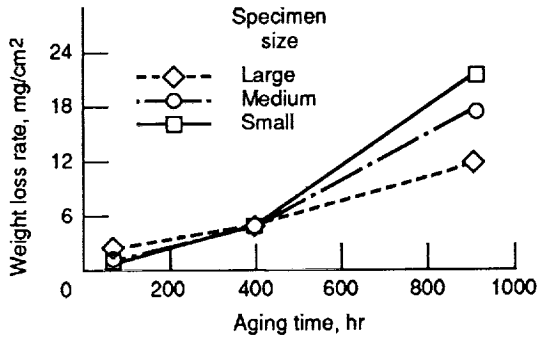

Figure 7.—Weight loss rate of T–40R-fiber-reinforced PMR–15 composites aged in air at 316 °C.

(a) Celion 6000.

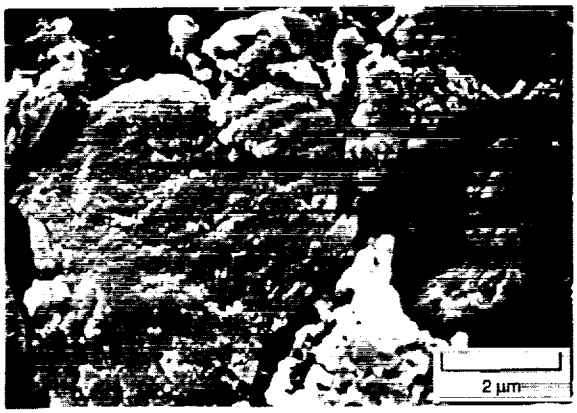

(b) T–40.

Figure 9.—End views (S3 surface) of graphite-fiber-reinforced PMR–15 composites after aging in air at 316 °C—greater magnifications of views shown in figure 8.

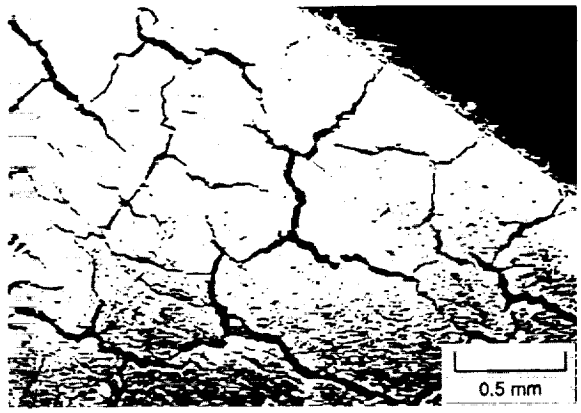

(a) Celion 6000/PMR–15 composite after 1212 hours.

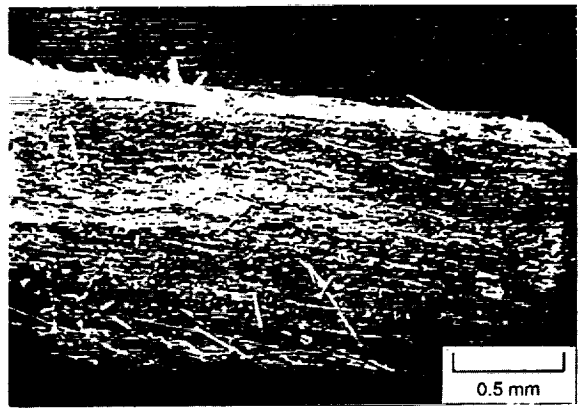

(b) T–40R/PMR–15 composite after 889 hours.

Figure 8.—End views (S3 surface) of graphite-fiber-reinforced PMR–15 composites after aging in air at 316 °C.

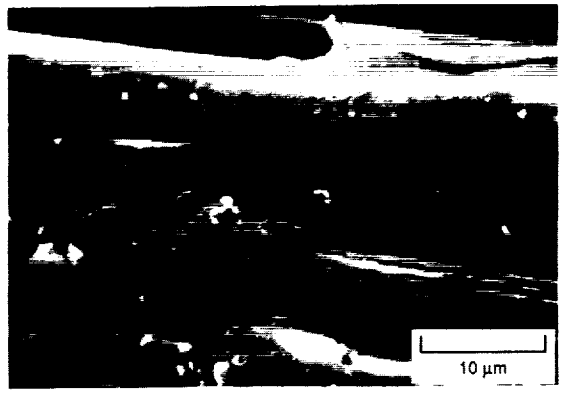

Figure 10.—Scanning electron micrograph of Celion 6000 fiber (S2 surface) after air aging in a PMR–15 composite.

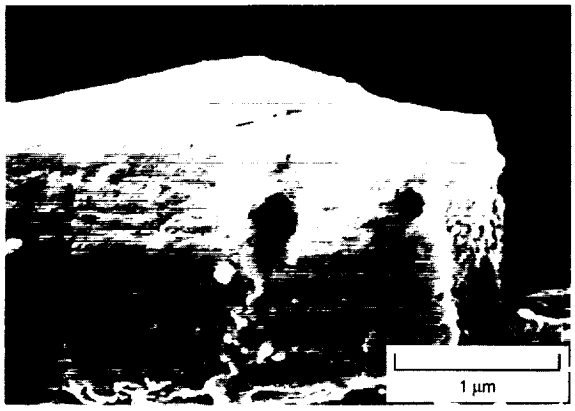

(a) Fiber ends (S3 surface).

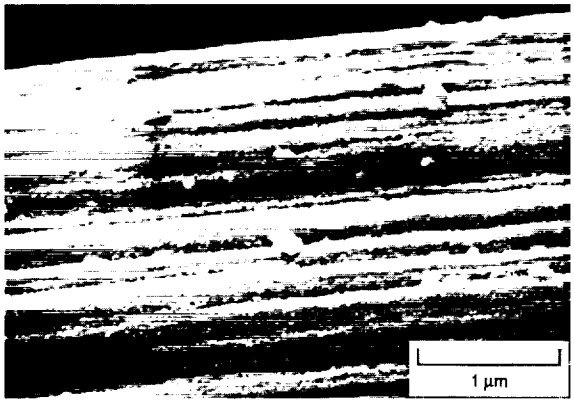

(b) Fiber circumferential surface (S2 surface).

Figure 11.—Celion 6000/PMR–15 composite aged in air at 316 °C. Fibers are from degraded outer layer but have not been directly exposed to air.

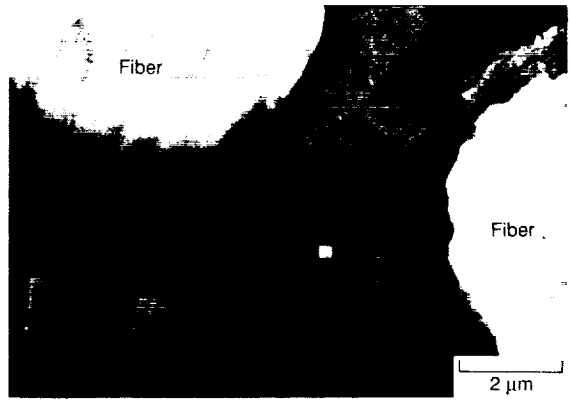

Figure 12.—End views (S3 surface) of T–40R/PMR–15 composite aged in air at 316°, showing selective oxidation of matrix.

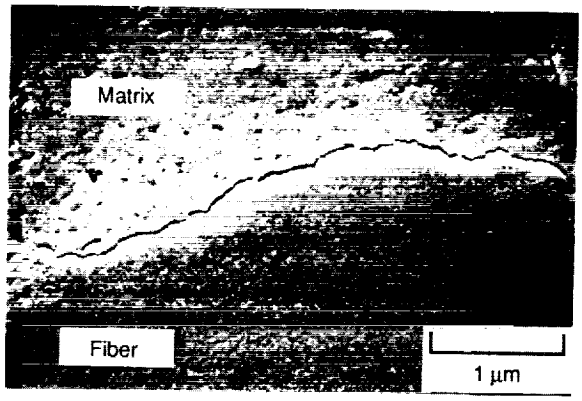

(a) Crack at interface.

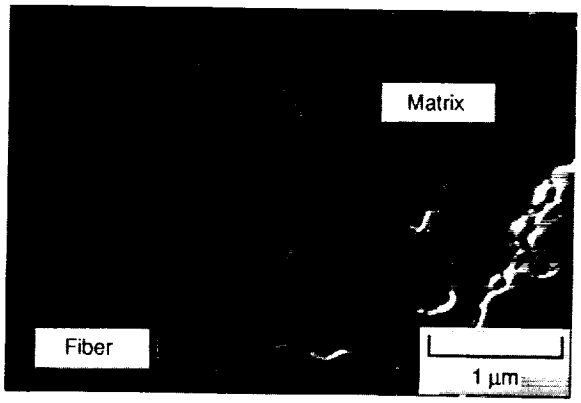

(b) Voids at interface.

Figure 13—T–40R composite interior material aged in air at 316 °C.

Figure 14.— Central portion of aged Celion 6000/PMR–15 composite specimen aged in air at 316 °C.

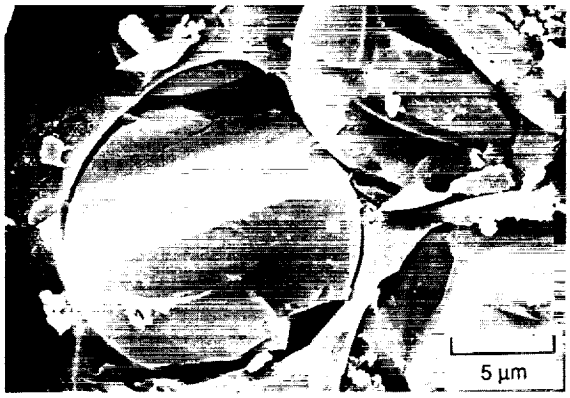

(a) Nicalon.

(b) Nextel 312.

Figure 15.—End views (S3 surfaces) of ceramic composites aged in air at 316°C, showing separations between fibers and matrix.

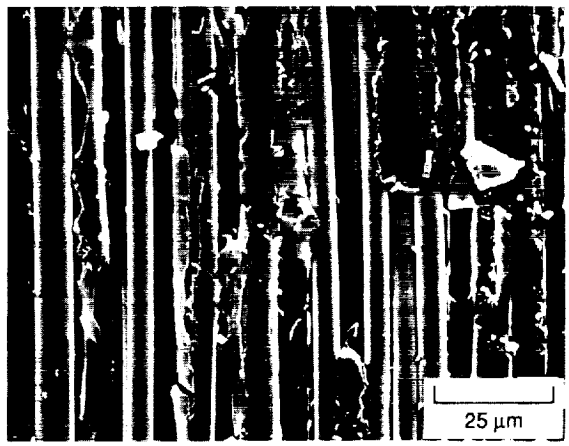

Figure 16.—Interior surface (S2 surface) of Nicalon composite produced by cleaving with a razor. No signs of good fiber-to-matrix bonding are visible. Fiber surfaces are clean.

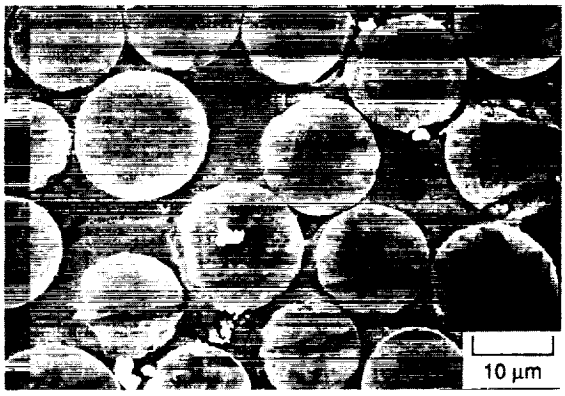

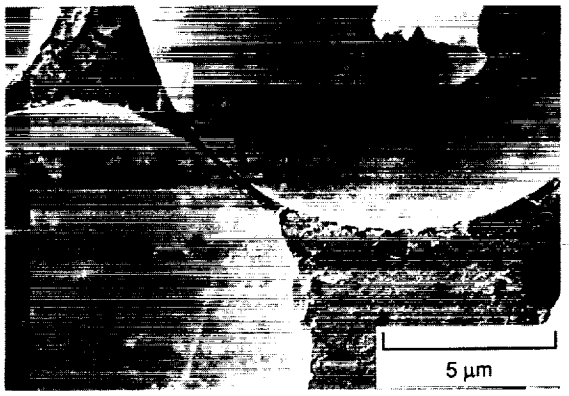

Figure 17.—Interior of Nicalon/PMR–15 composite aged in air at 316 °C. No fiber-matrix separations are visible.

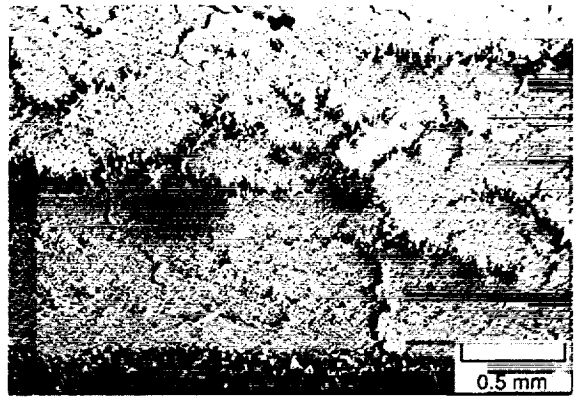

Figure 18.—End view (S3 surface) of Nextel 312-fiber-reinforced composite after aging in air at 316°C.

NASA
National Aeronautics and Space Administration

Report Documentation Page

1. Report No.	2. Government Accession No.	3. Recipient's Catalog No.
NASA TM-103648		

4. Title and Subtitle	5. Report Date
Effect of Fiber Reinforcements on Thermo-oxidative Stability and Mechanical Properties of Polymer Matrix Composites	6. Performing Organization Code

7. Author(s)	8. Performing Organization Report No.
Kenneth J. Bowles	E-5834
	10. Work Unit No. 505-01-01

9. Performing Organization Name and Address	11. Contract or Grant No.
National Aeronautics and Space Administration Lewis Research Center Cleveland, Ohio 44135-3191	13. Type of Report and Period Covered Technical Memorandum

12. Sponsoring Agency Name and Address	14. Sponsoring Agency Code
National Aeronautics and Space Administration Washington, D.C. 20546-0001	

15. Supplementary Notes

16. Abstract

A number of studies have investigated the thermo-oxidative behavior of polymer matrix composites. Two significant observations have been made from these research efforts. First, fiber reinforcement has a significant effect on composite thermal stability; second, geometric effects must be considered when evaluating thermal aging data. A number of studies that address these areas have been performed at the NASA Lewis Research Center. The information presented herein, a compilation of some results from these studies, shows the influence of the reinforcement fibers on the oxidative degradation of various polymer matrix composites. The polyimide PMR-15 was the matrix material that was used in these studies. The control composite material was reinforced with Celion 6000 graphite fiber. T-40R graphite fibers, along with some very stable ceramic fibers were selected as reinforcing fibers because of their high thermal stability. The ceramic fibers were Nicalon (silicon carbide) and Nextel 312 (alumina-silica-boron oxide). The mechanical properties of the two graphite fiber composites were significantly different, probably owing to variations in interfacial bonding between the fibers and the polyimide matrix. The Celion 6000/PMR-15 bond is very tight but the T-40/PMR-15 bond is less tight. Three oxidation mechanisms were observed. One involved the preferential oxidation of the Celion 6000 fiber ends at cut surfaces, leaving a surface of matrix material with holes where the fiber ends were originally situated; the second, preferential oxidation of the composite matrix; and the third, interfacial degradation by oxidation. The latter two mechanisms were also observed on fiber end cut surfaces. The fiber and interface attacks appeared to initiate interfiber cracking along these surfaces.

17. Key Words (Suggested by Author(s))	18. Distribution Statement
Composites; Polyimides; Aging; Graphite fiber; Ceramic fiber; Oxidation; Interfaces; Mechanical properties	Unclassified – Unlimited Subject Category 24

19. Security Classif. (of this report)	20. Security Classif. (of this page)	21. No. of pages	22. Price*
Unclassified	Unclassified	32	A03

NASA FORM 1626 OCT 86

*For sale by the National Technical Information Service, Springfield, Virginia 22161